communications physics
A Nature Portfolio journal

Article

https://doi.org/10.1038/s42005-026-02804-3

Circular ratchet currents in two dimensional tellurene with an asymmetric grating

M. D. Moldavskaya [1], L. E. Golub [2] ✉, Chang Niu [3,4], Peide D. Ye [3,4] & S. D. Ganichev [1,5]

Terahertz ratchet effect converts alternating electric fields into direct currents in low-dimensional systems with broken spatial symmetry and provide a route towards room-temperature terahertz optoelectronics. Here, we investigate the ratchet effect in two-dimensional tellurene, whose crystal structure is formed by helical atomic chains and exhibits intrinsic chirality. Terahertz excitation generates a circular ratchet photocurrent flowing along the chiral *c* axis, whose direction is controlled by the radiation helicity and reverses when the radiation helicity is switched from right- to left-handed circular polarization. The photocurrent is observed at room temperature over a broad range of gate voltages, with the Fermi level tuned from the conduction band near the Weyl point through the band gap and into the valence band, where the energy dispersion is nearly parabolic. A microscopic theory based on the Boltzmann kinetic equation reproduces the polarization and gate-voltage dependences of the photocurrent. Our results highlight a potential of tellurene based ratchet devices for helicity-sensitive terahertz photodetection.

Chirality is a profound and ubiquitous concept that permeates various realms of nature, manifesting itself in an extensive array of materials and phenomena. From the intricate molecular biology that underpins all living organisms to the fundamental principles of particle physics, chirality plays a pivotal role in shaping our understanding of the natural world. At its core, chirality refers to the unique spatial asymmetry found in certain structures that cannot be superimposed by any combination of rotation and translation. The significance of chirality goes beyond mere structural differences. There are also chirality-dependent chemical and physical properties, as well as different responses to external stimuli, see refs. 1–4 for reviews. In condensed matter physics, it is bulk tellurium and two-dimensional (2D) tellurene which are most well studied chiral materials[5–9]. An important example of an optoelectronic phenomenon in bulk tellurium are the circular photogalvanic and circular photon drag effects, where an electric current is driven by the light helicity[6,10,11]. Most recently, circular photogalvanic photocurrents have been also detected in two-dimensional (2D) tellurene[12,13]. The emergence of 2D Te-based structures provides an opportunity to study chirality-dependent optoelectronic phenomena, in which *extrinsic* chirality effects are produced by superimposing an asymmetrical grating on 2D tellurene samples, which creates ratchet structures. This unifies the physics of chiral materials with the ratchet effect—the generation of a DC electric current in response to an AC electric field in systems with broken inversion symmetry, for reviews see refs. 14–21. In this work, we propose and demonstrate that a THz electric field acting on an asymmetrical grating fabricated on a 2D tellurene sample can efficiently generate a ratchet current. The direction of this current reverses when the light helicity changes from left- to right-circular polarization. We also developed a microscopic theory describing the formation of this current for Weyl and parabolic energy bands, which are relevant for positive and negative back gate voltages applied to the tellurene layer.

Results

Basic concept

The proposed ratchet structure under study consists of a 2D tellurene conduction layer with a superimposed asymmetric lateral metallic grating, as shown in Fig. 1. The removal of spatial inversion in the structure is a necessary condition for the ratchet effect, and the asymmetrical lateral superlattice serves as an extrinsic source for this effect. The grating results in the electrostatic potential $V(x, y)$, acting on the electrons being periodic in the x direction with a period d: $V(x+d, y) = V(x, y)$. In equilibrium, the electrons occupy the potential minima, resulting in modulated electron density with a period d. When uniform THz radiation is normally incident

[1]Physics Department, University of Regensburg, Regensburg, Germany. [2]Institute of Theoretical Physics and Halle-Berlin-Regensburg Cluster of Excellence CCE, University of Regensburg, Regensburg, Germany. [3]Elmore Family School of Electrical and Computer Engineering, Purdue University, West Lafayette, Indiana, IN, USA. [4]Birck Nanotechnology Center, Purdue University, West Lafayette, Indiana, IN, USA. [5]CENTERA Labs, Institute of High Pressure Physics of the Polish Academy of Sciences, Warsaw, Poland. ✉e-mail: Leonid.Golub@physik.uni-regensburg.de

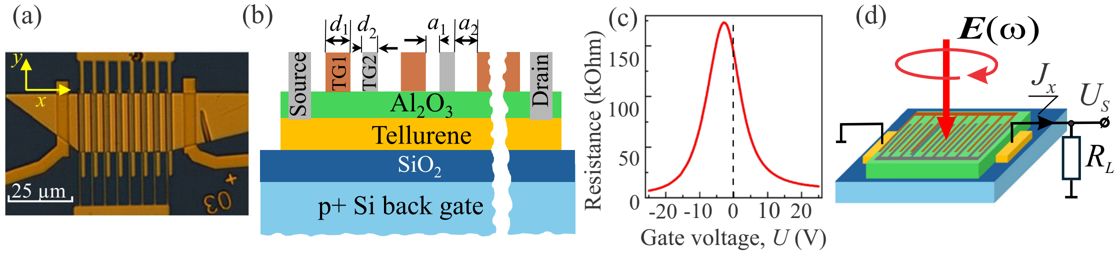

Fig. 1 | Ratchet devices and experimental arrangement. a, b Show an optical micrograph and a cross-section of the ratchet structure. Tellurene flake is deposited on top of $p+$ Si substrate covered by 90 nm SiO_2 layer. Nickel source and drain contacts with thickness of 50 nm were fabricated by electron beam evaporation on the short sides of the rectangular flakes, which were 46×23 μm^2. To cap the Te flakes, we deposited a 15-nm-thick layer of Al_2O_3. The asymmetric grating consists of supercells, each formed by two Ti stripes having widths d_1 = 1.5 and d_2 = 0.5 μm, spacings a_1 = 0.5 and a_2 = 2.5 μm, and thickness 50 nm. The supercell is repeated 8 times forming the asymmetric grating with the period $d = d_1 + a_1 + d_2 + a_2$. **c** Shows the two-point resistance as a function of the back gate voltage. **d** Sketches the experimental set-up.

on an asymmetric grating, an additional periodically modulated electric field is produced that acts on the electrons in the tellurene layer. This field is caused by the near field of diffraction and is enhanced in comparison with the far field of radiation. Consequently, the amplitude of the electric field, $\boldsymbol{E}(\boldsymbol{r},t) = \boldsymbol{e}E(\boldsymbol{r})\exp(-i\omega t) + c.c.$, is modulated in space with the same period: $E(x+d, y) = E(x, y)$. Here, $\boldsymbol{e}$ is the polarization vector, which can be complex for elliptical polarization, and ω is the radiation frequency. Note that the metallic grating does not act as a conventional diffraction grating in the far field because the grating period is much smaller than the THz wavelength. Instead, the grating produces a strongly nonuniform near-field distribution in the vicinity of the tellurene layer. This near-field modulation leads to a spatial modulation of the electric field amplitude $E(x, y)$. The modulation results in the simultaneous action of both the static and dynamic forces:

$$\boldsymbol{F}(\boldsymbol{r},t) = -\nabla V(\boldsymbol{r}) + e\boldsymbol{E}(\boldsymbol{r},t). \tag{1}$$

which causes the ratchet DC electric current. For the modulation period d much larger than the electron mean free path and for the photon energy and the potential size much smaller than the electron Fermi energy, we can use the kinetic theory for calculations of the ratchet currents. The Boltzmann equation for the distribution function $f(\boldsymbol{p}, \boldsymbol{r}, t)$ has the form

$$\frac{\partial f}{\partial t} + \boldsymbol{v_p}\cdot\frac{\partial f}{\partial \boldsymbol{r}} + \boldsymbol{F}(\boldsymbol{r},t)\cdot\frac{\partial f}{\partial \boldsymbol{p}} = \mathrm{St}[f]. \tag{2}$$

Here $\boldsymbol{v_p} = \partial\varepsilon_{\boldsymbol{p}}/\partial\boldsymbol{p}$ is the group velocity of electrons with the momentum $\boldsymbol{p}$ and energy $\varepsilon_{\boldsymbol{p}}$, St is the collision integral, and the force acting on the electrons is a sum of the static and time-oscillating terms, Eq. (1). In order to get the ratchet current we iterate the kinetic Eq. (2) in small perturbations V and E and find the DC correction to the distribution function $\delta f(\boldsymbol{p}, \boldsymbol{r}) \propto E^2\nabla_{x,y}V$. Then the current density is calculated as

$$\boldsymbol{j} = eg_sg_v\sum_{\boldsymbol{p}}\boldsymbol{v_p}\,\overline{\delta f(\boldsymbol{p},\boldsymbol{r})}, \tag{3}$$

where the factors g_s and $g_v = 2$ account for the spin and valley degeneracy in tellurene ($g_s = 1$ for the valence band and $g_s = 2$ for the conduction band), and the line denotes averaging over coordinates. Consequently, the ratchet current is proportional to the components $\Xi_{x,y}$ of the lateral asymmetry parameter

$$\Xi = \overline{E^2(\boldsymbol{r})\nabla V(\boldsymbol{r})}. \tag{4}$$

Despite both the static force $-\nabla V$ and the radiation intensity I modulation $\propto E^2$ have zero mean values, their averaged product Ξ is nonzero in the studied structure. Figure 1a shows that the structure has the lowest possible symmetry, C_1, without any nontrivial symmetry elements. In particular, the structure is chiral because it has no mirror reflection planes, and both components Ξ_x and Ξ_y are nonzero. The symmetry analysis shows that the DC electric current can be driven by circularly-, linearly-polarized or unpolarized radiation

$$j_x = \Xi_y\gamma P_{\mathrm{circ}} + \Xi_x(\chi_L P_L + \chi_0) + \Xi_y\tilde{\chi}_L\tilde{P}_L. \tag{5}$$

Here P_{circ} is the radiation helicity, and P_L, $\tilde{P}_L$ are the Stokes parameters defining the degrees of the linear polarization[22], and the factors $\gamma, \chi_L, \tilde{\chi}_L, \chi_0$ describe the circular, linear and polarization-independent ratchet effects, respectively. These factors are independent of the periodic potential and radiation intensity, being determined by the properties of 2D carriers in tellurene and radiation frequency. As an important result, the first term in Eq. (5) shows that the helicity-driven ratchet current in tellurene-based devices is expected in the direction x corresponding to the chiral axis c.

THz-induced circular ratchet currents

To demonstrate that the circular ratchet effect emerges in tellurene-based devices, we fabricated an asymmetric metal interdigitated grating formed by two combs having different stripe widths and separations. The grating was deposited on a tellurene flake covered by Al_2O_3 for electrical isolation, see Fig. 1 and section Methods. When designing the grating, we considered the following arguments: (i) To excite the ratchet effect, the grating period must be much smaller than the radiation wavelength. (ii) It should possess strong asymmetry to provide an asymmetric near-field distribution. (iii) The stripes should be thick enough to be opaque and support near-field formation. (iv) It should be easy to fabricate using technology. Sweeping the back gate voltage U shows that the charge neutrality point (CNP) is observable in the two-point resistance, as seen in Fig. 1c. Tellurene-based devices were excited by normal-incident radiation of THz pulsed laser (100 ns pulses, 1 Hz repetition rate) operating at frequencies f = 1.07 and 2.02 THz, see Fig. 1d. We used a $\lambda/4$ plate to excite ratchet currents sensitive to radiation helicity. By rotating the plate, we varied the THz radiation helicity according to $P_{\mathrm{circ}} \propto \sin 2\varphi$[22,23], where $\varphi = 0$ is the angle between the laser polarization plane and the optical axis of the plate. Note that for $\varphi = 0$, the radiation is linearly polarized, with the electric field vector $\boldsymbol{E}$ tilted from the y-direction by about 15°. Figures 2 and 3 show the electric current $J_x = U_s/R_L$ obtained for different effective gate voltages $U_G = U - U_{\mathrm{CNP}}$, when applying radiation at a frequency of 1.07 THz. The current is excited along the c-axis, which is perpendicular to the grating stripes. We used a $\lambda/4$ plate to excite ratchet currents sensitive to radiation helicity. By rotating the plate, we varied the THz radiation helicity according to $P_{\mathrm{circ}} \propto \sin 2\varphi$[22,23], where $\varphi = 0$ is the angle between the laser polarization plane and the optical axis of the plate. Note that for $\varphi = 0$, the radiation is linearly polarized, with the electric field vector $\boldsymbol{E}$ tilted from the y-direction by about 15°. Figures 2 and 3 show the data obtained for different effective gate voltages when applying radiation at a frequency of 1.07 THz.

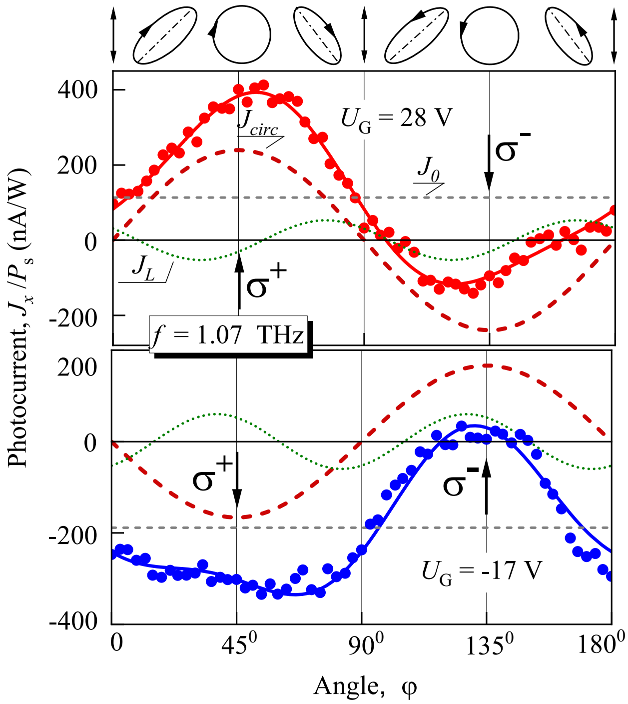

Fig. 2 | Helicity-driven ratchet current in tellurene excited by the radiation with frequency $f = 1.07$ THz. The normalized photocurrent, J_x/P_s, as a function of the lambda-quarter rotation angle, φ. The data are shown for a radiation frequency f = 1.07 THz and several effective back gate voltages ranging from hole- ($U_G < 0$) to electron-conductivity ($U_G > 0$). The solid lines represent the corresponding fits according to Eq. (6). The individual contributions, J_{circ}, J_0, and J_L, are plotted by the brown, gray, and green dashed lines, respectively. The fitting coefficients are plotted in Fig. 4 and S4 of Supplementary Note 1. Vertical arrows indicate the right- (σ^+) and left-handed (σ^-) circular polarizations, and the ellipses on top illustrate the polarization states at various angles φ.

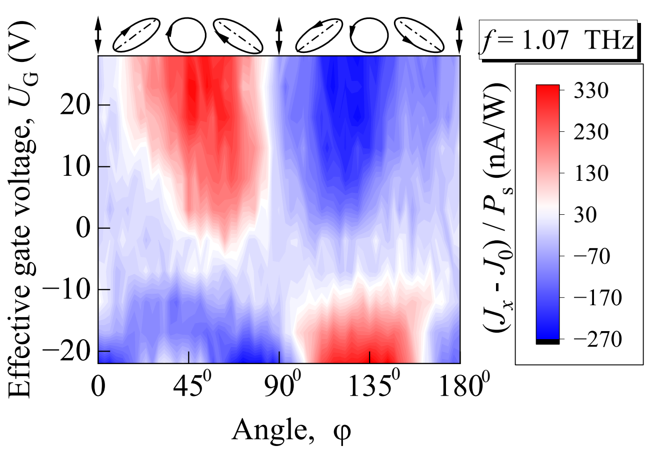

Fig. 3 | Color map of the gate-dependent ratchet current. Phase angle φ and effective gate voltage dependencies of the color-coded photocurrent strength $(Jx - J_0)/P_s$ as a function of the angle φ. The data are obtained for f = 1.07 THz.

As a central result, Figs. 2 and 3 reveal that the photocurrents excited by right (σ^+) and left (σ^-) circularly-polarized radiation have substantially different amplitudes. We find that the total photocurrent is well fitted by above derived Eq. (5), which for the used setup takes the form

$$J_x = J_{\rm circ} \sin(2\varphi) + J_0 + J_{\rm L} \sin 4(\varphi + \varphi_0) \tag{6}$$

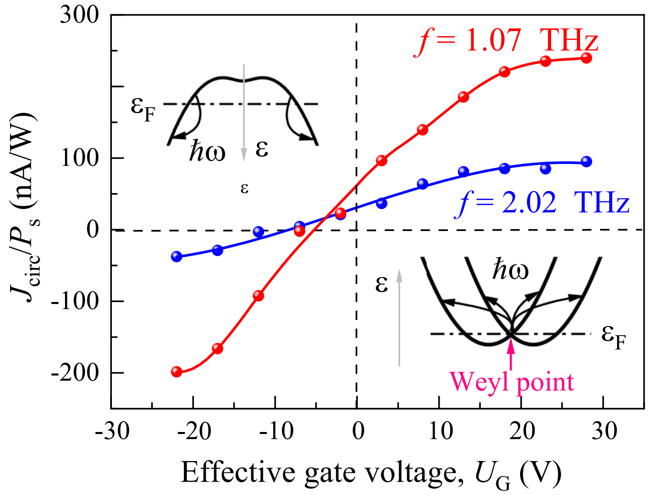

Fig. 4 | Helicity-driven ratchet current in the valence and conduction bands. Dependencies of the circular photocurrent excited by radiation with frequencies f = 1.07 and f = 2.02 THz on the effective gate voltage U_G. The solid lines are guides for eyes. Insets sketches indirect (Drude-like) optical transitions in the valence (left, negative gate voltages) and conduction (right, positive gate voltages) energy bands.

where $J_{\rm circ} \propto \Xi_y \gamma$ is the amplitude of the circular photocurrent, J_0 is the amplitude of the polarization-independent contribution, J_L is the amplitude of the photocurrent in response to linearly polarized radiation, and φ_0 is the phase shift. In this equation we have merged both linear ratchet currents using that, in the current setup, the Stokes parameters take form $P_L = (1 + \cos 4\varphi)/2$ and $\tilde{P}_L = \sin 4\varphi$[23]. Figures 2 and 3 reveal the dominance of the circular photocurrent over the linear one. Importantly, in the reference sample without grating, the circular photocurrent is absent, see Fig. S1 in the Supplementary Note 1.

The dependence of the circular ratchet current on the effective gate voltage is shown in Fig. 4. It reveals that the current reverses its direction at small negative effective gate voltages. By varying the radiation intensity, we observed that the current changes according to $J_x \propto E^2$, as shown in Fig. S2 in Supplementary Note 1. Similar behavior is detected for radiation with a frequency about twice as high, f = 2.02 THz, but with an essential contribution of the linear current J_L over the entire range of gate voltages, see Figs. 4 and 5, as well as Figs. S3 and S5 in Supplementary Note 1.

Discussion

Before discussing the results and presenting our developed theory of ratchets, we will briefly address the possible competing mechanisms of circular photocurrent that are sensitive to the rotational direction of the electric field of the radiation, $\boldsymbol{E}$. According to symmetry arguments, such a current is only permitted in gyrotropic systems. In the structures under study, this condition is met for unstructured tellurene and for tellurene with an asymmetric grating on top. Our experiments demonstrate that the photocurrent in unstructured tellurene flakes is insensitive to radiation helicity (see Fig. S1 in the Supplementary Note 1). Conversely, the ratchet structure fabricated on a tellurene flake yields a strong current whose direction reverses when the radiation helicity is reversed. This indicates the effective chirality of the complete tellurene-plus-grating structure. A frequently addressed mechanism of photocurrent formation in graphene grating structures, similar to those studied here, is the thermoelectric effect. Indeed, thermoelectric effects[24,25] may in the structures with grating cause polarization-independent current (J_0) due to the Seebeck ratchet, see e.g., refs. 26,[27], and may also contribute to the linear ratchet effect (J_L). However, the circular current can hardly be attributed to the thermoelectric effect. The theory of the ratchet effect, which is a radiation-induced direct current in

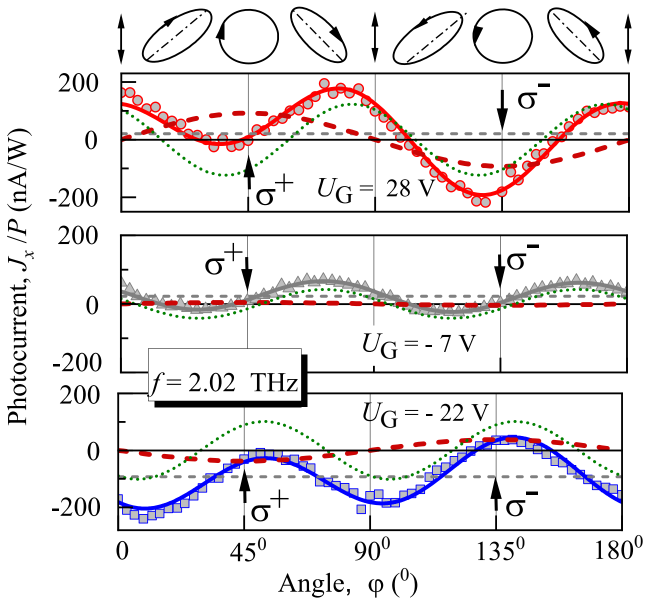

Fig. 5 | Helicity-driven ratchet current observed at f = 2.02 THz. Dependencies of the photocurrent (colored symbols) excited by radiation with f = 2.02 THz on the rotation angle φ of the $\lambda/4$ wave plate. The data are shown for several effective back gate voltages ranging from hole ($U_G < 0$) to electron conductivity ($U_G > 0$). The photoresponse is normalized to the laser power P_s incident on the sample. The vertical arrows in each panel mark the right-handed (σ^+) and left-handed (σ^-) circular polarization states, respectively. The solid lines represent the corresponding fits according to Eq. (6). The individual contributions, J_{circ}, J_0, and J_L, are plotted by the brown, gray, and green dashed lines, respectively. The fit coefficients are plotted in Figs. 4 and S5 of Supplementary Note 2. Note that the circular photocurrent contribution is negligible for gate voltages close to the CNP.

periodically modulated structures with built-in asymmetry, demonstrates that circularly polarized radiation gives rise to a photocurrent sensitive to radiation handedness in a tellurene-plus-grating structure.

The focus of our work is the ratchet current in tellurene-based devices, which can be illustrated by the following model. The radiation electric field changes the spatially-modulated distribution of electrons resulting in the new, nonequilibrium modulation profile which is formed after a quarter of the period $\pi/(2\omega)$. At this moment, the electric field vector of the circularly polarized radiation is already rotated by 90° from the initial direction, accelerating the electrons. After a half of the period, the situation tends to reverse, however, the electrons are bunched in the other parts of the spatially modulated structure, where the electric field amplitude has another value. As a result, the compensation does not take place giving rise to the DC ratchet current. Remarkably, at opposite circular polarization, the acceleration occurs in the opposite direction, and the circular ratchet current $J_{circ} \propto P_{circ}$ reverses. This is the mechanism of the circular ratchet effect.

Following on from the theory developed above, the ratchet current scales linearly with the radiation intensity $I \propto E^2$ as observed in experiments, see Fig. S2 in Supplementary Note 1. The gate voltage dependence of the circular ratchet current is presented in Fig. 4. Depending on the gate voltage U_G, the Fermi level lies in the conduction band, valence band or in the band gap, see insets in Fig. 4. The conduction band which is relevant for transport at large positive U_G, consists of two Rashba-splitted subbands in each tellurene valley. At the bottom of conduction band, a Weyl point in the 2D bandstructure is present. Consequently, we deal with Weyl fermions at a range of positive gate voltages, and with an almost parabolic energy dispersion at negative voltages. The linear (Weyl-like) dispersion is relevant only close to the Weyl point at relatively small positive gate voltages, whereas at sufficiently high positive gate voltages the dispersion deviates from the linear regime and becomes approximately parabolic. As it is difficult to determine which disorder scattering mechanism is realized in our structure, we consider both short- and long-range Coulomb scattering.

To understand the observed circular ratchet current behavior upon variation of the gate voltage and radiation frequency, we develop the microscopic theory of the effect. We show that the circular ratchet current

$$j_x^{\rm circ} = \gamma \Xi_y P_{\rm circ} \tag{7}$$

is strongly sensitive to the type of both 2D energy dispersion of charge carriers and the disorder scattering potential. First we consider parabolic energy dispersion $\varepsilon_{\boldsymbol{p}} = p^2/(2m)$. At degenerate statistics for the short-range (SR) disorder scattering potential we obtain (see Supplementary Note 2 for derivation)

$$\gamma^{\rm SR} = \frac{e^3\tau^2}{2\pi\hbar^2 m\omega[1+(\omega-\omega_{\rm pl}^2/\omega)^2\tau^2]}. \tag{8}$$

Here τ is the transport scattering time, and $\omega_{pl} = sq$ is the 2D plasmon frequency with $q = 2\pi/d$ and s being the plasmon wavevector and velocity, respectively. For the short-range disorder, τ is independent of the Fermi energy ε_F. For long-range Coulomb (Coul) disorder scattering potential we get

$$\gamma^{\rm Coul} = \gamma^{\rm SR}\frac{3\Omega^6+29\Omega^4+4\Omega^2+32}{(1+\Omega^2)(\Omega^2+4)^2}, \tag{9}$$

where $\Omega = \omega\tau$, and $\tau \propto \varepsilon_F$.

For the linear energy dispersion $\varepsilon_{\boldsymbol{p}} = v_0 p$, relevant to the vicinity of the Weyl point (at small positive U_G), the expressions for γ^{SR} and γ^{Coul} take form

$$\gamma_{\rm lin}^{\rm Coul} = \frac{e^3\tau^2 v_0^2/(\pi\hbar^2\varepsilon_F\omega)}{(1+\omega^2\tau^2)[1+(\omega-\omega_{\rm pl}^2/\omega)^2\tau^2]}, \tag{10}$$

$$\gamma_{\rm lin}^{\rm SR} = -\gamma_{\rm lin}^{\rm Coul}\frac{\Omega(2\Omega^4+\Omega^2+8)}{(\Omega^2+4)^2}. \tag{11}$$

Here, $\tau \propto \varepsilon_F$ for Coulomb scattering and $\tau \propto 1/\varepsilon_F$ for short-range scattering. In the above equations the charge has a sign (negative for electrons and positive for holes), therefore, variation of the gate voltages via the charge neutrality point results in the change of sign of the ratchet current.

The above equations show that the ratchet current is strongly enhanced by plasmonic effects in the frequency range close to the 2D plasmon. Owing to the lateral superlattice superimposed onto the tellurene, excitation of the plasmons becomes possible. In ref. 28, it was shown that the circular ratchet effect is dramatically enhanced in the vicinity of plasmonic resonances, see Eq. (8). Using $q = 2\pi/d$ and $s = \sqrt{eU_G/m}$, we estimated the plasmon frequency to be $\omega_{pl}/(2\pi) \approx 0.6$ THz at $U_G = 10$ V. We found that this value remains below the THz frequencies used in the present work. Thus, the experiments are performed in the regime of $\omega_{pl} < \omega$, and we consider the non-resonant ratchet effects. Under this assumption, the dependencies of γ on the Fermi energy are shown in Fig. 6 for two energy dispersions and short-range and Coulomb disorder potentials. It is seen from Fig. 6 that the circular ratchet current is strongly sensitive to both the type of energy dispersion and details of disorder scattering.

The experiments presented in this work are performed at room temperature. At a sufficiently low U_G when the resistance has a maximum, the Fermi level lies in the band gap. Consequently, the free carriers are described by the Boltzmann statistics, and the circular ratchet current (7) is determined by

$$\gamma^{\rm SR}(T) = \gamma^{\rm SR}\frac{N\pi\hbar^2}{mk_B T}, \tag{12}$$

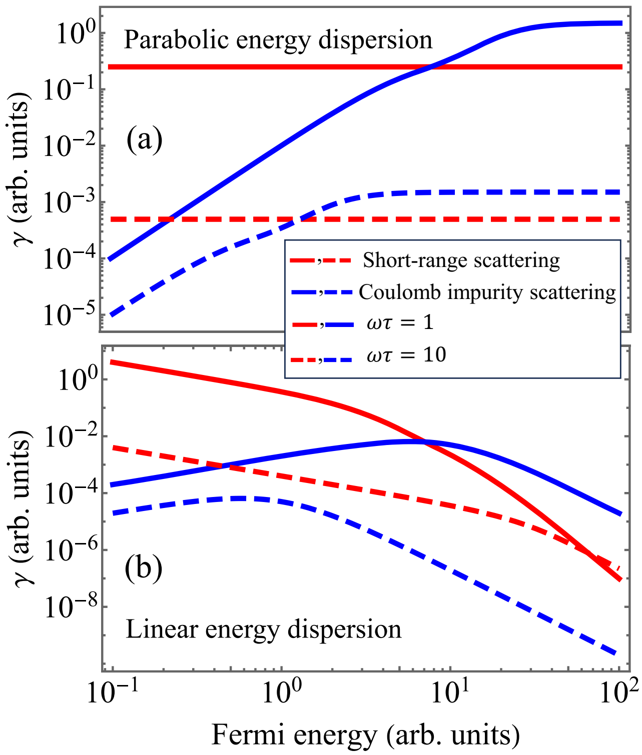

Fig. 6 | Calculated Fermi energy dependence of the circular ratchet current amplitude |γ|. The current amplitude describes the behavior when the Fermi level lies deep in the conduction or valence band. Parabolic (**a**) and linear (**b**) energy dispersions and two elastic scattering mechanisms are considered. Solid and dashed curves are for $\omega\tau = 1$ and 10, respectively.

where γ^{SR} is the value (8), N is the charge density, T is the temperature, and k_B is the Boltzmann constant. For the linear energy dispersion this relation (between $\gamma^{SR}_{lin}(T)$ and γ^{SR}_{lin}) also holds.

The gate voltage dependence of the circular ratchet amplitude presented in Fig. 4 follows from the theory presented above. At a sufficiently low U_G the free carriers have Boltzmann statistics, and it follows from Eqs. (8) and (12) that $\gamma \propto N$, therefore, the circular ratchet current monotonously increases with $|U_G|$. This is true for both positive and negative U_G provided the Fermi level is in the band gap. At high $|U_G|$, by contrast, the carriers are degenerate. Note that in this case both electrons and holes have almost parabolic energy dispersion (passing through the Weyl point in the electronic dispersion does not result in significant changes to the ratchet current). Then, according to Fig. 6a, γ is a constant for short-range disorder or saturates for Coulomb scattering with increase of ε_F. In both cases the linear increase of the circular ratchet current amplitude changes to a weaker dependence on U_G. Exactly this behavior takes place at high positive U_G for both frequencies used in the experiments, see Fig. 4.

The theory also explains the observed change of the circular ratchet current sign upon variation of the gate voltage clearly seen in Fig. 4. Indeed, Eqs. (8) and (10) reveal that the current is proportional to the third power of the carrier charge, which changes in the vicinity of the CNP. The slight shift of the zero point of the current from the CNP to negative gate voltages we attribute to the fact that electrons still substantially contribute to the current. This is because both electrons and holes are present at a small U_G, and the photocurrent of the electrons dominates that of the holes.

Conclusions

To summarize, we observed that the lateral asymmetric grating fabricated on top of the 2D tellurene induces a circular ratchet current in the chiral axis direction c. An important feature of chirality is the sensitivity of material property to the radiation helicity. Our experiments demonstrate that the photocurrent in unstructured tellurene flakes, as studied here, is insensitive to the radiation helicity. At the same time the ratchet structure fabricated on the tellurene flake yields a strong current whose direction reverses when the radiation helicity is reversed. This indicates the effective chirality of the complete tellurene-plus-grating structure. Due to the near-field diffraction, the grating periodically modulates the electric field of the incident radiation. Furthermore, the grating produces the periodic electrostatic potential. The developed semiclassical theory demonstrates that the combined action of these fields on 2D carriers results in the DC helicity-driven electric current. The DC current is controlled by the back gate voltage. The obtained Fermi energy dependence of the circular ratchet current describes well the experimental data for both positive and negative gate voltages. In the former case, the current is carried by the chiral Weyl fermions, while in the latter case it is formed in the valence band with almost parabolic dispersion. The current is detected at technologically important room temperature which paves the way for development of novel electronic devices. As a future task, since the circular ratchet current is controlled by the lateral asymmetry parameter, we expect that its magnitude can be substantially magnified by finding a special design that increases the value of the lateral parameter Ξ. Moreover, tuning the structure parameters and radiation frequency to plasmonic resonance should result in the resonant circular current. Study the photocurrent dependence of the system as a function of U_{TG1} and U_{TG2} would help clarify whether thermoelectric effects induced by the asymmetric top gate structure, alike in multigate graphene structures[26,27], contribute to the response of the tellurene ratchets. Furthermore, decreasing the structure period and temperature would allow for a superlattice period smaller than the mean free path. This results in the formation of minibands, and in the new mechanisms of the circular ratchet current formation in the quantum-mechanical regime. As an outlook, it is worth performing comparative measurements with opposite crystal handedness, mirrored gratings, or current measured perpendicular to the c-axis.

Methods

Figure 1a, b show the photograph and cross-section of the studied devices, respectively. The 2D Te flakes were synthesized using the hydrothermal growth method[29]. The synthesized 2D Te flakes, which had a thickness of approximately 30 nm, were rinsed twice in water before being transferred to a 90-nm SiO_2/Si substrate using the Langmuir-Blodgett method. This substrate served as a back gate. In the following, the long side of the tellurene bar is oriented along the c-axis of the tellurium (x-direction) and short sides along a-axis (y-direction). To cap the Te flakes, we deposited a 15-nm-thick layer of Al_2O_3 on top using atomic layer deposition with $(CH_3)_3Al$ (TMA) and H_2O as precursors at 200 °C.

Asymmetric grating was formed by two combs having different stripe widths and separations, see Fig 1. The asymmetric grating consists of supercells, each formed by two Ti stripes having widths $d_1 = 1.5$ and $d_2 = 0.5$ µm, spacings $a_1 = 0.5$ and $a_2 = 2.5$ µm, and thickness 50 nm. The supercell period is $d = d_1 + a_1 + d_2 + a_2$. During the measurements, the grating electrodes were electrically floating. Despite the presence of the 15 nm Al_2O_3 spacer, the metallic fingers modify the local electrostatic environment and produce an effective periodic modulation of the electronic potential.

To demonstrate that the circular photocurrent is caused by exclusively the ratchet effect, we additionally fabricated tellurene flakes with the same technology, but without grating. The experiments described above were performed at room temperature. To change the concentration and carrier type, a voltage U is applied to the back gate. For the investigated devices, the CNP was found at negative gate voltages of approximately -3 V, see Fig. 1c. For subsequent analysis, the back gate voltage is presented as an effective voltage, $U_G = U - U_{CNP}$, where U_{CNP} is the voltage at which the CNP appears. Electron and hole-type conductivity occur for positive and negative U_G, respectively, as described in ref. 30. The carrier concentration for an effective gate voltage of ± 20 V is about 5×10^{12} cm^{-2}. The mobility μ extracted from the two-terminal gate-dependent transport measurements are about 520 and 200 cm^2/Vs for holes and electrons, respectively. The source (drain) contact resistance for Te at on state is about 1–5 Ohm mm[31], which is about 50–250 Ohm in our current device. This is negligible compared to the channel resistance, see Fig. 1c. The corresponding Fermi energies are approximately equal to 55 meV for electrons and 45 meV for holes which justifies the assumptions employed in the kinetic theory.

As a source of radiation we used optically pumped pulsed NH_3 laser operated at f = 1.07 THz (λ = 280 µm, $\hbar\omega$ = 4.4 meV) and 2.02 THz (λ = 148 µm, $\hbar\omega$ = 8.35 meV). The laser generated single pulses with a duration of about 100 ns and a repetition rate of 1 Hz. The radiation with $f \approx 1.07(2.02)$ THz and power $P \approx 10(30)$ kW was focused in a spot of about 5 (3.8) mm diameter. Taking into account the area of the device, $S_{device} \approx 10^{-5}\,cm^2$, we obtain that the power irradiating the sample $P_s = P \times (S_{device}/S_{spot}) \approx 0.5(2.7)$ W, where S_{spot} is the beam spot area. The induced photocurrents were detected as a voltage drop across load resistors R_L = 50 Ohm. The signals were recorded using digital oscilloscopes.

Data availability

The data that support the findings of this study are available from the corresponding author upon request.

Received: 26 February 2026; Accepted: 29 July 2026;
Published online: 06 August 2026

References

1. Crassous, J. et al. Materials for chiral light control. *Nat. Rev. Mater.* **8**, 365 (2023).
2. Zhu, H. & Yakobson, B. I. Creating chirality in the nearly two dimensions. *Nat. Mater.* **23**, 316 (2024).
3. Matassa, R., Ray, S. C. & Zheng, Y. Chirality in nanomaterials. *Sci. Rep.* **14**, 26268 (2024).
4. Habibović, D., Hamilton, K. R., Neufeld, O. & Rego, L. Emerging tailored light sources for studying chirality and symmetry. *Nat. Rev. Phys.* **6**, 663 (2024).
5. Calavalle, F. et al. Gate-tuneable and chirality-dependent charge-to-spin conversion in tellurium nanowires. *Nat. Mater.* **21**, 526 (2022).
6. Moldavskaya, M. D. et al. Photocurrents in bulk tellurium. *Phys. Rev. B.* **108**, 235209 (2023).
7. Sławińska, J. Spin selectivity in elemental tellurium and other chiral materials. *Appl. Phys. Lett.* **123**, 240504 (2023).
8. Joseph, N. B., Bandyopadhyay, A. & Narayan, A. Chirality-tunable nonlinear Hall effect. *Chem. Mater.* **36**, 8602 (2024).
9. Suárez-Rodríguez, M. et al. Odd nonlinear conductivity under spatial inversion in chiral tellurium. *Phys. Rev. Lett.* **132**, 046303 (2024).
10. Asnin, V. M. et al. Observation of a photo-emf that depends on the sign of the circular-polarization of the light. *JETP Lett.* **28**, 74 (1978).
11. Shalygin, V. A., Moldavskaya, M. D., Danilov, S. N., Farbshtein, I. I. & Golub, L. E. Circular photon drag effect in bulk tellurium. *Phys. Rev. B* **93**, 045207 (2016).
12. Niu, C. et al. Tunable chirality-dependent nonlinear electrical responses in 2D tellurium. *Nano Lett.* **23**, 8445 (2023).
13. Mönch, E. et al. Terahertz radiation driven nonlinear transport phenomena in two-dimensional tellurene. *Nano Lett.* **25**, 476 (2024).
14. Linke, H. Ratchets and brownian motors: basics, experiments and applications. *Appl. Phys. A.* **75**, 167 (2002).
15. Reimann, P. Brownian motors: noisy transport far from equilibrium. *Phys. Rep.* **361**, 57 (2002).
16. Hänggi, P. & Marchesoni, F. Artificial brownian motors: controlling transport on the nanoscale. *Rev. Mod. Phys.* **81**, 387 (2009).
17. Ivchenko, E. L. & Ganichev, S. D. Ratchet effects in quantum wells with a lateral superlattice. *JETP Lett.* **93**, 673 (2011).
18. Denisov, S., Flach, S. & Hänggi, P. Tunable transport with broken space–time symmetries. *Phys. Rep.* **538**, 77 (2014).
19. Bercioux, D. & Lucignano, P. Quantum transport in Rashba spin–orbit materials: a review. *Rep. Prog. Phys.* **78**, 106001 (2015).
20. Cubero, D. & Renzoni, F. Hidden symmetries, instabilities, and current suppression in brownian ratchets. *Phys. Rev. Lett.* **116**, 010602 (2016).
21. Reichhardt, C. J. O. & Reichhardt, C. Ratchet effects in active matter systems. *Annu. Rev. Condens. Matter Phys.* **8**, 51 (2017).
22. Saleh B. E. A. & Teich, M.C. *Fundamentals of Photonics* (John Wiley and Sons Ltd., 2019).
23. Bel'kov, V. V. et al. Magneto-gyrotropic photogalvanic effects in semiconductor quantum wells. *J. Phys. Condens. Matter* **17**, 3405 (2005).
24. Song, J. C. W., Rudner, M. S., Marcus, C. M. & Levitov, L. S. Hot carrier transport and photocurrent response in graphene. *Nano Lett.* **11**, 4688–4692 (2011).
25. Castilla, S. et al. Fast and sensitive terahertz detection using an antenna-integrated graphene pn junction. *Nano Lett.* **19**, 2765 (2019).
26. Olbrich, P. et al. Terahertz ratchet effects in graphene with a lateral superlattice. *Phys. Rev. B.* **93**, 075422 (2016).
27. Delgado-Notario, J. A. et al. Enhanced terahertz detection of multigate graphene nanostructures. *Nanophotonics* **11**, 519 (2022).
28. Rozhansky, I., Kachorovskii, V. & Shur, M. Helicity-driven ratchet effect enhanced by plasmons. *Phys. Rev. Lett.* **114**, 246601 (2015).
29. Qiu, G. et al. Quantum Hall effect of Weyl fermions in n-type semiconducting tellurene. *Nat. Nanotechnol.* **15**, 585 (2020).
30. Niu, C. et al. Tunable circular photogalvanic and photovoltaic effect in 2d tellurium with different chirality. *Nano Lett.* **23**, 3599 (2023).
31. Wang, Y. et al. Field-effect transistors made from solution-grown two-dimensional tellurene. *Nat. Electron.* **1**, 228 (2018).

Author contributions

M.D.M. carried out the experiments with the help from S.D.G. L.E.G. developed the theory. C.N. and P.D.Y. fabricated devices. S.D.G. conceived and supervised the project. M.D.M., L.E.G. and S.D.G. prepared the manuscript with input from all authors. All authors contributed to the discussion and analysis of the results.

Funding

The financial support of the Deutsche Forschungsgemeinschaft (DFG, German Research Foundation) via Project-IDs 564981228 (MO 5219/1-1) and 521083032 (GA 501/19) is gratefully acknowledged. Work of L.E.G. was funded by the German Research Foundation (DFG) as part of the German Excellence Strategy – EXC3112/1 – 533767171 (Center for Chiral Electronics). S.D.G. is grateful for the support of by the European Union through the ERC-ADVANCED grant TERAPLASM No. 101053716. Views and opinions expressed are, however, those of the author(s) only and do not necessarily reflect those of the European Union or the European Research Council Executive Agency. Neither the European Union nor the granting authority can be held responsible for them. Open Access funding enabled and organized by Projekt DEAL.

Competing interests

The authors declare no competing interests.

Additional information

Supplementary information The online version contains supplementary material available at https://doi.org/10.1038/s42005-026-02804-3.

Correspondence and requests for materials should be addressed to L. E. Golub.

Peer review information *Communications Physics* thanks Igor Rozhansky, Sylvain Massabeau, Felix Hernandez and the other, anonymous, reviewer for their contribution to the peer review of this work.